Bone 120 (2019) 439–445

Contents lists available at ScienceDirect

Bone

journal homepage: www.elsevier.com/locate/bone

Full Length Article

Cortical porosity assessment in the distal radius: A comparison of HR-pQCT measures with Synchrotron-Radiation micro-CT-based measures

Nikoo Soltan[a], Chantal E. Kawalilak[a], David M. Cooper[b], Saija A. Kontulainen[c], James D. Johnston[a,*]

[a] Department of Mechanical Engineering, University of Saskatchewan, Saskatoon, SK, Canada
[b] Department of Anatomy & Cellular Biology, University of Saskatchewan, Saskatoon, SK, Canada
[c] College of Kinesiology, University of Saskatchewan, Saskatoon, SK, Canada

ARTICLE INFO

Keywords:
Cortical porosity
Distal radius
HR-pQCT
SR-μCT
Synchrotron radiation

ABSTRACT

Objective: To determine the agreement between cortical porosity derived from high resolution peripheral quantitative computed tomography (HR-pQCT) (*via* standard threshold, mean density and density inhomogeneity methods) and synchrotron radiation micro-CT (SR-μCT) derived porosity at the distal radius.
Methods: We scanned 10 cadaveric radii (mean donor age: 79, SD 11 years) at the standard distal region using HR-pQCT and SR-μCT at voxel sizes of 82 μm and 17.7 μm, respectively. Common cortical regions were delineated for each specimen in both imaging modalities. HR-pQCT images were analyzed for cortical porosity using the following methods: Standard threshold, mean density, and density inhomogeneity (*via* recommended and optimized equations). We assessed agreement in porosity measures between HR-pQCT methods and SR-μCT by reporting predicted variance from linear regression and mean bias with limits of agreement (LOA).
Results: The standard threshold and mean density methods predicted 85% and 89% of variance and indicated underestimation (mean bias −9.1%, LOA −15.9% to −2.2%) and overestimation (10.4%, 4.6% to 16.2%) of porosity, respectively. The density inhomogeneity method with recommended equation predicted 89% of variance and mean bias of 14.9% (−4.3 to 34.2) with systematic over-estimation of porosity in more porous specimens. The density inhomogeneity method with optimized equation predicted 91% of variance without bias (0.0%, −5.3 to 5.2).
Conclusion: HR-pQCT imaged porosity assessed with the density inhomogeneity method with optimized equation indicated the best agreement with SR-μCT derived porosity.

1. Introduction

Porosity in bone is associated with bone fragility and fracture risk and is an indicator of osteoporosis progression [1,2]. Though the degeneration of bone has traditionally been linked with the deficit of trabecular bone, the significant role of cortical porosity (Ct.Po) in quantifiably marking bone loss and fragility has recently been recognized [1,3–5]. The advent of imaging technologies that are capable of non-invasive detection of Ct.Po have been invaluable; however, there remains significant room for improving the accuracy of these measurements.

Currently, Ct.Po of peripheral bones can be measured *in vivo* using high resolution peripheral quantitative computed tomography (HR-pQCT) [3,6,7]. The standard HR-pQCT evaluation of Ct.Po utilizes a threshold-based method which separates pores from bone tissue in a binary way using a global bone density threshold [6]. Additionally, density-based methods, which utilize principles of partial volume averaging to derive porosity from bone mineral density (BMD), have been proposed [8,9]. Recently, Iori et al. [10] proposed a new method which incorporates BMD inhomogeneity to estimate Ct.Po, specifically *via* BMD mean, standard deviation, and full width at half maximum from BMD histograms. In this work, they acquired high-resolution *ex vivo* images of the proximal femur, virtually down-sampled the data to mimic *in vivo* HR-pQCT settings, then derived model equations for estimating Ct.Po *in vivo*.

Though conventional HR-pQCT offers the advantage of non-invasively measuring bone micro-architecture, it is constrained by its resolution (first generation HR-pQCT I: 82 μm voxel size; second-generation HR-pQCT II: 61 μm voxel size) and is affected by imaging artifacts which can limit the accuracy of its measurements [11].

* Corresponding author at: Department of Mechanical Engineering, University of Saskatchewan, 57 Campus Drive, Saskatoon, SK S7N5A9, Canada.
E-mail address: jd.johnston@usask.ca (J.D. Johnston).

https://doi.org/10.1016/j.bone.2018.12.008
Received 29 August 2018; Received in revised form 9 December 2018; Accepted 10 December 2018
Available online 13 December 2018

Synchrotron radiation micro-CT (SR-μCT) imaging is ideal for *ex vivo* examination of bone micro-architecture, including Ct.Po. The monochromatic x-ray source of SR-μCT offers images unaffected by beam hardening artifacts and the high signal-to-noise ratio contributes to high contrast and high spatial resolution (*e.g.*, 17.7 μm voxel size) [12]. SR-μCT has been proposed as the gold-standard for the analysis of cortical bone micro-architecture [13–15], and thus it is ideal for validating proposed HR-pQCT methods for estimating Ct.Po.

Previous work by Jorgenson et al. [8] and Ostertag et al. [16] compared HR-pQCT and SR-μCT-derived cortical micro-architecture, including Ct.Po, in isolated sections of distal tibia specimens. Iori et al. [10] compared HR-pQCT and scanning acoustic microscopy (SAM) derived Ct.Po in isolated sections of the proximal femur. Evidence from the distal radius is needed to complement these findings from the tibia and femur. The distal radius is one of the most common fracture sites in postmenopausal women [17,18], and thus, a clinically relevant site assessed by HR-pQCT. The validity of HR-pQCT to measure bone micro-architecture, specifically Ct.Po, at the distal radius has yet to be determined. Importantly, micro-architectural properties from the distal tibia and proximal femur may not be directly comparable to the properties at the distal radius due to the smaller size of the distal radius, thinner metaphyseal cortex, and thus relatively greater challenges to capture micro-architectural properties, such as cortical porosity [19,20]. Also, as the inhomogeneity equations developed by Iori et al. [10] were based upon virtually down-sampled *ex vivo* image data, it is unclear whether the recommended model coefficients can be applied with true HR-pQCT image data acquired using *in vivo* settings.

The objective of this study was to evaluate the agreement between HR-pQCT-derived Ct.Po (*via* standard threshold, density-based, and inhomogeneity methods) and SR-μCT Ct.Po at the human distal radius.

2. Methods

2.1. Specimens

Ten intact embalmed cadaveric arms (5 male, 3 female, 2 unknown; mean age: 79 ± 11 years) were obtained from the University of Saskatchewan Anatomy and Cell Biology Bequeathal Program. The specimens had varying levels of intact soft tissue. No information was provided on the cause of death or medical history of the individuals. All procedures for the use of these specimens were approved by the University of Saskatchewan Biomedical Research Ethics Board. To facilitate the synchrotron imaging process, forearms were potted mid-shaft in bone cement (polymethylmethacrylate, PMMA), as per Edwards and Troy [21].

2.2. HR-pQCT scanning

The specimens were imaged using the first generation HR-pQCT scanner (HR-pQCT I; XtremeCT, Scanco Medical, Brüttisellen, Switzerland) at the standard distal region of the radius (9.02 mm scanned region of interest located 9.5 mm proximal to the reference line placement positioned at the mid-region of the radial endplate). The *in vivo* scanning protocol was provided by the manufacturer and is described elsewhere [22]. The HR-pQCT scans were reconstructed with an isotropic, nominal voxel size of 82 μm. Quality control of the HR-pQCT images used the manufacturer provided hydroxyapatite (HA)-based phantom of 0, 100, 200, 400 and 800 mg HA/cm^3 density rods and beam hardening was corrected using manufacturer-derived algorithms during scan reconstruction.

2.3. SR-μCT scanning

Using a similar position as the HR-pQCT scanning, the specimens were scanned by SR-μCT at the Canadian Light Source (Saskatoon, SK, Canada) using the Biomedical Imaging and Therapy (BMIT) Insertion Device (05ID-2, SOE-1) beamline. The sample stage was 200 mm from the detector (VHR90 Photonic Science). The scanning energy was set to 55 keV to be comparable with the HR-pQCT energy of 60 keV. Exposure times were between 0.13 and 0.24 s and 2250 projections were obtained over an angular range of 180°. Images were reconstructed using NRecon (Bruker microCT) at an isotropic voxel size of 17.7 μm. The use of 17.7 μm was determined to be the smallest voxel size possible while maintaining a large field of view to capture the full radius bone for comparison and matching to the HR-pQCT scans. Density calibrations were performed by scanning the previously mentioned HR-pQCT HA phantom under the same SR-μCT specimen scanning conditions.

2.4. Image analysis

2.4.1. Volume of interest

The volume of interest (VOI) for this study was defined as the 36 proximal HR-pQCT slices out of the full standard distal scan region (110 slices). The 36 proximal HR-pQCT slices corresponded to approximately 167 SR-μCT slices. To ensure that the same VOI was analyzed across both imaging modalities, the HR-pQCT and SR-μCT images were visually registered at the defined VOI.

2.4.2. Cortex characterization

To avoid manual segmentation error due to operator bias, we utilized a peeling approach to delineate a common cortical region for both HR-pQCT and SR-μCT images. In images from both imaging modalities, we defined comparable cortices by peeling off voxels radially inwards from the bone periosteal contour. A constant thickness was derived for each specimen in the defined VOI (Fig. 1).

To derive the ideal peel level for each specimen, first, using the standard manufacturer *in vivo* evaluation protocol [22], the HR-pQCT images were segmented and analyzed to obtain cortical outcomes, including Ct.Po, in the defined VOI. Next, through the Scanco Medical Image Processing Language (IPL), the HR-pQCT VOI for each specimen was peeled at different levels iteratively (starting with the sample average cortical thickness as the initial peel level) and evaluated for Ct.Po. The peel level that had the closest Ct.Po value to the Ct.Po acquired from manual segmentation of cortical bone in the HR-pQCT images was selected to define the ideal peel level. The mean percent difference in Ct.Po at the ideal peel level and the manually segmented cortex was 16%. The mean percent difference between the ideal peel level and the average manually segmented cortical thickness was 25%.

2.4.3. Cortex segmentation

Using Fiji [23] (a package distribution of ImageJ), periosteal contours for both the HR-pQCT and SR-μCT images were obtained using a global threshold of 400 mg HA/cm^3 (the Scanco Medical prescribed *in vivo* threshold for HR-pQCT). The contour line was manually corrected where it strayed from the periosteal boundary. Starting at the defined periosteal contour, the endocortical contour for both HR-pQCT and SR-μCT images was defined using the ideal peel level (as determined earlier) for each specimen throughout the entire VOI (Fig. 2). The boundary between the periosteal and endocortical contours defined the cortex.

2.5. Measured outcomes

We used Fiji image analysis to determine bone micro-architecture [23]. HR-pQCT Ct.Po was calculated using threshold, density-based, and inhomogeneity methods. SR-μCT Ct.Po was calculated using the threshold-based method as the gold-standard comparison.

2.5.1. Threshold-based Ct.Po

Cortical pores were identified using threshold-based segmentation of bone tissue. The HR-pQCT images were analyzed using the manufacturer prescribed standard threshold of 400 mg HA/cm^3. The SR-μCT

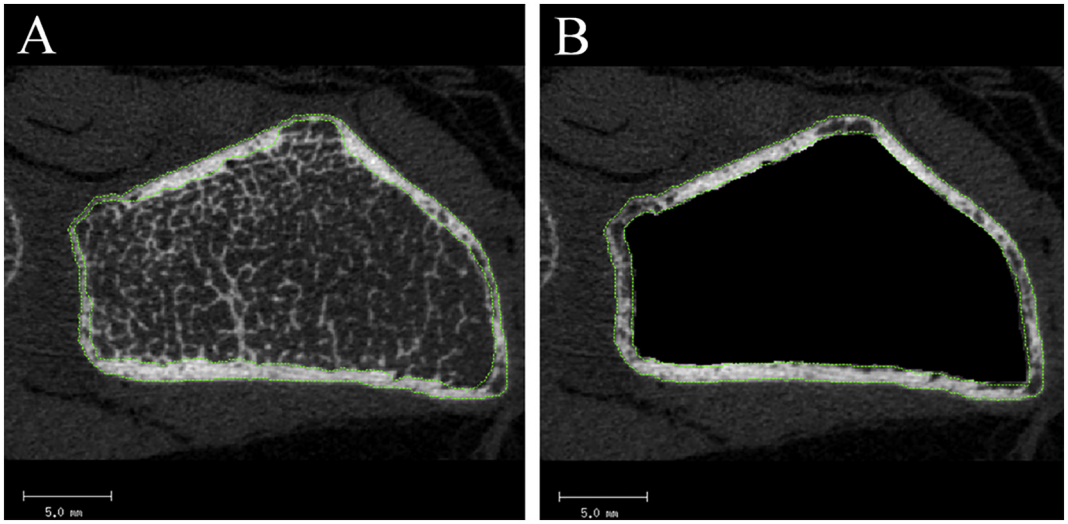

Fig. 1. A: Standard segmentation of cortex. B: Cortex segmented using a constant thickness peel level.

images were analyzed at a threshold of 750 mg HA/cm^3 [8]. Through thresholding, Ct.Po was determined *via* Eq. 1 [8].

$$\text{Ct. Po [\%]} = \left(1 - \frac{\text{bone volume}}{\text{total volume}}\right) * 100\% \quad (1)$$

2.5.2. Density-based Ct.Po

Using the principle of partial volume averaging, Ct.Po can be calculated from average BMD (BMD_{MEAN}) of each specimen *via* Eq. 2 [8]. BMD_{MEAN} was obtained by converting the average gray scale attenuation of the segmented VOI to units of mg HA/cm^3 using the phantom-based calibration for each imaging modality. The BMD of pure cortical bone was set to 1200 mg HA/cm^3.

$$\text{Ct. Po [\%]} = \left(1 - \frac{BMD_{MEAN}}{1200 \text{ mg HA/cm}^3}\right) * 100\% \quad (2)$$

2.5.3. Inhomogeneity-based Ct.Po – recommended equation

Using the methodology proposed by Iori et al., Ct.Po was calculated for each specimen *via* Eq. 3, described in detail in [10]. BMD measures included in the equation were BMD_{MEAN}, standard deviation (BMD_{SD}) and full width at half maximum from specimen histograms (BMD_{WIDTH}). These measures were included in the model as each was correlated with Ct.Po. The specific model coefficients pertain to *in vivo* imaging using HR-pQCT with a voxel size of 82 µm. Although the equation provided by Iori et al. [10] refers to local BMD measures, it can also be applied to the whole specimen (personal communication with Dr. Iori).

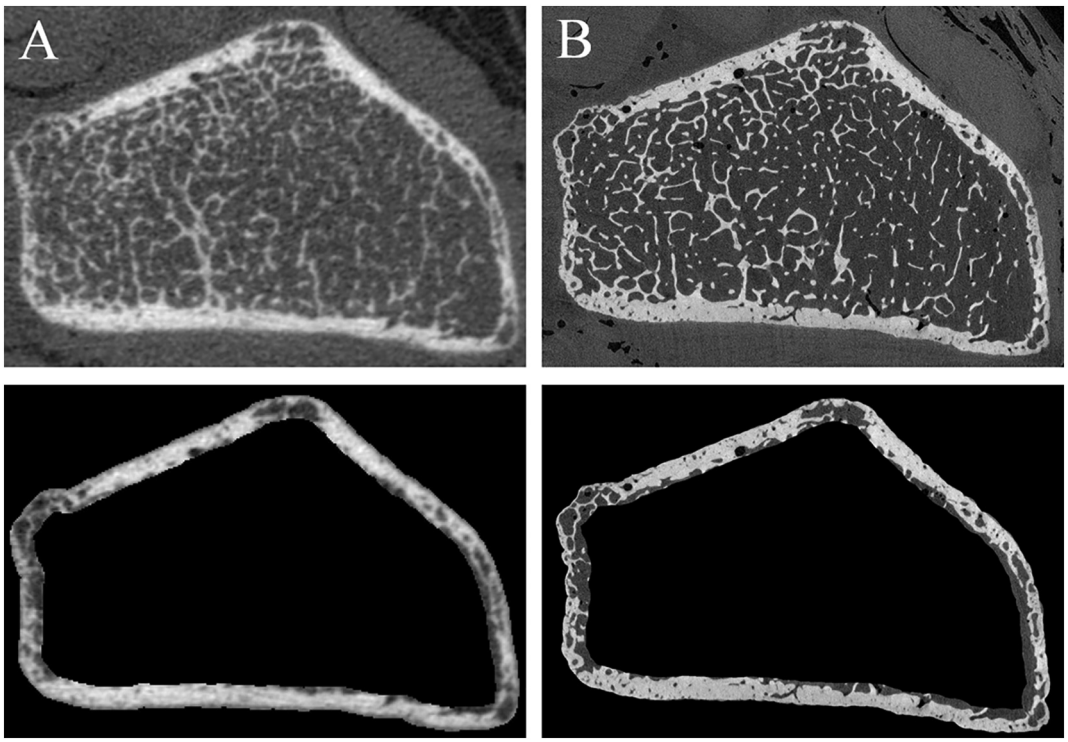

Fig. 2. Cortex segmentation using peeling. A: HR-pQCT, B: SR-µCT.

$$\text{Ct. Po [\%]} = 49.48\% - (0.0542\text{BMD}_{\text{MEAN}} - 0.0397\text{BMD}_{\text{SD}} - 0.0359\text{BMD}_{\text{WIDTH}}) \quad (3)$$

2.5.4. Inhomogeneity-based Ct.Po – optimized equation

As Eq. 3 provided by Iori et al. [10] was derived from virtually down-sampled *ex vivo* HR-pQCT image data, we sought to derive coefficients based upon actual HR-pQCT images acquired using *in vivo* settings. For this we used multiple linear regression with HR-pQCT based BMD_{MEAN}, BMD_{SD}, and $\text{BMD}_{\text{WIDTH}}$ as predictors of SR-μCT based Ct.Po. The derived coefficients are found in Eq. 4.

$$\text{Ct. Po [\%]} = 57.52\% - (0.0552\text{BMD}_{\text{MEAN}} - 0.0229\text{BMD}_{\text{SD}} - 0.0075\text{BMD}_{\text{WIDTH}}) \quad (4)$$

2.6. Statistical analysis

We used linear regression and Bland-Altman plots to assess the agreement between HR-pQCT-derived (threshold, density-based, and inhomogeneity methods) Ct.Po and SR-μCT derived Ct.Po. We report coefficient of variation (R^2) to assess variance in SR-μCT porosity predicted by HR-pQCT methods, and mean bias with 95% Limits of Agreement (LOA) for the Ct.Po difference calculated as [HR-pQCT − SR-μCT].

3. Results

The standard threshold-based Ct.Po explained 85% of variance in SR-μCT derived Ct.Po (Fig. 3A). Bland-Altman plots indicated that the standard threshold-based method under-estimated Ct.Po by −9.1% (95% LOA from −15.9% to −2.2%) in comparison to SR-μCT-derived Ct.Po (Fig. 3B).

Density-based Ct.Po explained 89% of variance in SR-μCT-derived Ct.Po (Fig. 3C). The density-based method over-estimated Ct.Po by +10.4% (LOA from 4.6% to 16.2%) in comparison to SR-μCT-derived Ct.Po (Fig. 3D).

The inhomogeneity method with the recommended equation for HR-pQCT explained 89% of variance in SR-μCT-derived Ct.Po (Fig. 3E). The mean bias was +14.9% (LOA from −4.3% to 34.1%) in comparison to SR-μCT-derived Ct.Po (Fig. 3F). Bland Altman plots indicated a proportional bias, illustrating an over-estimation of Ct.Po with more porous specimens (Fig. 3F).

The inhomogeneity method with the optimized equation explained 91% variance in SR-μCT-derived Ct.Po (Fig. 3G). The method showed no bias (bias 0.0%, LOA from −5.3% to −5.2%), when compared to SR-μCT-derived Ct.Po (Fig. 3H).

4. Discussion

The objective of this study was to evaluate the agreement between HR-pQCT-derived Ct.Po (*via* standard threshold, density-based, and inhomogeneity methods) and SR-μCT Ct.Po at the human distal radius. This is the first study to validate HR-pQCT Ct.Po measures of the intact distal radius. Our results indicated good agreement across HR-pQCT methods of Ct.Po and SR-μCT derived porosity; however, the inhomogeneity method with the optimized equation indicated the best agreement by explaining 91% of variance in gold-standard SR-μCT Ct.Po, and indicated no bias in porosity when compared to SR-μCT.

Using the standard threshold method, our results indicated ~9% under-estimation of Ct.Po. This under-estimation can be attributed to the imaging resolution limitations of the HR-pQCT where, due to the resolution dependences of the threshold method, HR-pQCT is unable to resolve all of the pores detected by SR-μCT.

Using the density-based method, our results indicated ~10% over-estimation of Ct.Po. This discrepancy may be explained, in part, by partial volume averaging at interfaces separating bone from surroundings of lower density (*e.g.*, soft tissue, air) in HR-pQCT images. This averaging would lower the average BMD and result in the over-estimation of Ct.Po. Conversely, partial volume effects are likely less prominent in SR-μCT images due to greater resolution and contrast.

Using the inhomogeneity approach with the recommended equation for HR-pQCT proposed by Iori et al. [10], our results indicated ~15% bias with a proportional over-estimation of Ct.Po in specimens with higher porosity. Iori et al. [10] scanned sections of the proximal femur with the second generation HR-pQCT (HR-pQCT II) and validated the BMD-based method of deriving Ct.Po by comparing down-sampled *ex vivo* HR-pQCT II images to high-resolution reference values measured with SAM. The discrepancy between our findings and those by Iori et al. [10] could be attributed to: 1) their equation being derived from virtually down-sampled *ex vivo* HR-pQCT II image data (*vs.* actual HR-pQCT I image data with *in vivo* settings); 2) differences in micro-architecture between the distal radius and proximal femur [10]; 3) differences between the HR-pQCT I and II (*e.g.*, image noise, contrast); as well as 4) Ct.Po accuracy of the employed SAM modality (discussed in more detail below). To address these issues, we sought to derive optimized equation coefficients using actual HR-pQCT I image data of the distal radius with *in vivo* settings. The optimized equation offered no over- or under-estimation of Ct.Po when compared to SR-μCT. It could be argued that the optimized equation is simply tuned to match our specific data. However, given that our model coefficients agree with that of Iori et al. [10] (*e.g.*, their coefficient for BMD_{MEAN} was 0.0542, ours was 0.0552), this indicates that the inhomogeneity method appears valid, but is not necessarily calibrated for HR-pQCT I or the distal radius.

Throughout this study, the gold-standard SR-μCT Ct.Po was calculated using a threshold of 750 mg HA/cm^3. The SR-μCT threshold was used as per the analysis conducted previously by Jorgenson et al. [8]. We also verified the validity of this threshold using various line-profiles with the half-maximum height method [24,25]. For reference, we found that our correlation coefficients for the threshold method had little dependence on the SR-μCT threshold. Specifically, an SR-μCT threshold of 750 mg HA/cm^3 ± 30% varied our correlation coefficients by approximately ± 3%. As such, we believe the Ct.Po measurements offered by SR-μCT are valid.

Previous validation research has compared HR-pQCT Ct.Po measures with SR-μCT based Ct.Po of the tibia [8,16] and SAM based Ct.Po of the proximal femur [10]. Similar to our findings, past SR-μCT studies showed good Ct.Po agreement between the two imaging modalities. Jorgenson et al. [8] also reported that the standard threshold method under-estimated Ct.Po while the density-method over-estimated Ct.Po, with comparable regression lines and LOA to those reported here. Altogether, these results indicate that the applied threshold and density-based HR-pQCT methods are not site-specific (*i.e.*, are valid for multiple sites). The reported higher goodness of fit ($R^2 = 0.98$) between HR-pQCT threshold and density-based Ct.Po with SR-μCT-derived Ct.Po by Jorgenson et al. [8] may be attributed to the different regions of analysis and SR-μCT scanning resolutions. Jorgenson et al. [8] studied small isolated samples of the tibia (mid-shaft) with prominently cortical regions which differ from the micro-architecture of the radius in the standard clinical scan region. Also, due to the resolution dependence of the threshold method, the discrepancy in results could be attributed to the different SR-μCT scanning resolutions used in our respective studies. In contrast to previous SR-μCT research, our findings did not agree with prior SAM-based research. Specifically, Iori et al. [10] reported that the standard threshold method under-estimated Ct.Po with higher degree of under-estimation at higher porosities, which contrasts with our findings. We believe this is due to differences in Ct.Po measures offered by SR-μCT and SAM. For the same threshold-based HR-pQCT estimate of Ct.Po, SAM appears to offer a Ct.Po measure ~2.5× that of SR-μCT, likely explaining observed discrepancy [8,10]. Although SR-μCT has been proposed as the gold-standard for the analysis of cortical bone

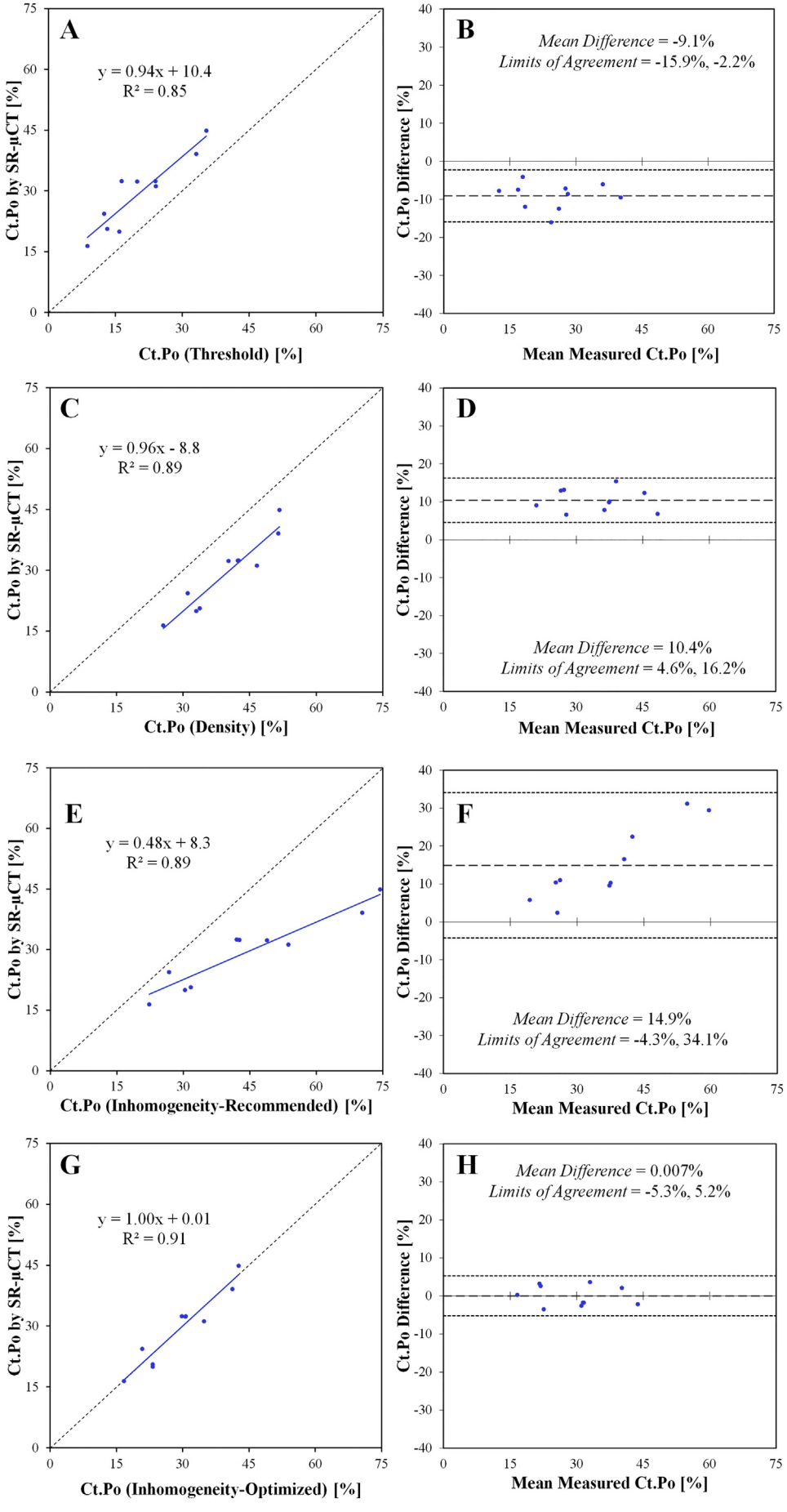

(caption on next page)

Fig. 3. Linear regression and Bland-Altman plots for comparing SR-μCT Ct.Po with HR-pQCT Ct.Po derived from the standard threshold method (A, B), density-method (C, D), inhomogeneity method with recommended equation (E, F), and inhomogeneity method with optimized equation (G, H).

micro-architecture [13–15], further research would benefit comparing SR-μCT and SAM based estimates of Ct.Po.

The strengths of this study pertain to the specimen type, region of analysis, segmentation approach and the consistency of analysis across both HR-pQCT and SR-μCT images. First, the use of intact distal radii can provide representative attenuations obtained through *in vivo* imaging. Second, our region of analysis offers relevant results as it corresponds to the standard HR-pQCT scanning region conducted *in vivo*. Third, to delineate common cortical regions between both imaging modalities, a peeling approach was used. This is important as segmenting cortical regions for this analysis has conventionally involved some degree of manual segmentation which adds error due to operator bias. A few studies have used isolated segments of bone from the mid-shaft region (which contains predominantly cortical bone) and have treated the entire segment as cortical bone, eliminating the need for segmentation [8,16]. Though this method eliminates errors from operator subjectivity, it is not practical with the standard distal radius region where the cortical-trabecular interface is less distinct. The peeling method enabled the analysis of the standard HR-pQCT region which contains both cortical and trabecular bone while eliminating the subjectivity of conventional semi-automatic segmentation. Fourth, as outlined in the methods section, the ideal peel level for each specimen was derived from Ct.Po obtained from manual segmentation of the cortex in the HR-pQCT images. This approach ensured that our porosity distributions were representative of those reported in population based studies [26]. Fifth, to ensure image analysis consistency, we applied the following approaches: the same analysis program was used for both imaging modalities; the standard manufacturer provided HR-pQCT phantom was used for the calibration of both imaging modalities; efforts were taken to replicate *in vivo* scanning conditions; and the partially intact radii were imaged in a similar orientation as *in vivo* scanning conditions in order to replicate comparable beam hardening artifacts.

Though efforts were made to minimize sources of error, this study was faced with limitations which present opportunities for improvement. First, the generalizability of our results could be improved by using a larger sample size. Second, the visual registration of HR-pQCT and SR-μCT images could have introduced some error in identifying the common VOIs. Previous studies have used image registration to identify common VOIs in different image modalities. However, registration is subject to interpolation artifacts that could skew the density distribution in the samples [11]. Because we ensured similar scanning orientations and regions, we believe that visually registering common regions offered reasonable accuracy. Additionally, the visual registration was conducted by one operator to prevent inter-operator error. Third, our analysis in this study was limited to a proximal region of the standard HR-pQCT scan site. Though our decision to focus on the proximal region of the distal radius was due to the prominence of a larger cortical region, future work should assess the full standard/clinical scan region of the HR-pQCT. Fourth, to delineate the cortical regions using peeling, the contour of the periosteal border was manually corrected where the contour strayed from the border. Though contouring the periosteal border involves less ambiguity than the endosteal border, this manual correction may have created differences in the contour between the images of the same bone. However, these errors were minimized since one operator conducted the contouring. Fifth, although the peeling method eliminated the subjectivity of conventional semi-automatic segmentation, it did not account for varying cortical thickness throughout the distal radius. For reference, we elected to use a peel approach due to the time-consuming and highly subjective nature of manually segmenting the endosteal boundary in each SR-μCT slice. An alternative, less time-consuming approach would have been to define the endosteal boundary using spline-fit contour lines every 5th slice, which could then be interpolated for the whole SR-μCT image volume (every 5th slice since there were ~5 times more SR-μCT slices than HR-pQCT slices). Although this approach may have introduced error due to different SR-μCT and HR-pQCT spline-fit contour lines, it would have accounted for a degree of varying cortical thickness throughout the distal radius. This is a direction of future research. Sixth, in this study we applied the same HR-pQCT and SR-μCT image processing methodology as Jorgenson et al. [8]. We did this for the purpose of comparing and verifying study findings with prior research. This approach though omitted post-processing filtering of HR-pQCT image data used to enhance structural accuracy and contrast (*e.g.*, Laplace-Hamming filtering [27]). Such filtering may have altered (for better or worse) agreement between SR-μCT and HR-pQCT estimates of Ct.Po. This is also a direction of future research. Seventh, the strengths of correlations determined in this study are likely affected by the donor age and sex. Our specimens were from older donors representing a clinically relevant population for cortical porosity assessment. However, it would be prudent to repeat this study with larger number of specimens from female and male donors with wider age range and information of osteoporosis diagnosis.

This study was faced with additional technical limitations. First, it was limited by the SR-μCT scanning resolution. Though an isotropic voxel size of 10 μm or smaller is considered to give the most consistent Ct.Po measurements [7], this is difficult to attain for the large fields of view required to image partially intact forearms. Second, although the peeling approach utilized in this study allowed for the analysis of the standard clinical region, the analysis was very time intensive. Deriving the ideal peel level from the HR-pQCT images involved analyzing each individual specimen at several peel thicknesses. Due to the specimen dependence, the practicality of this method (especially for larger sample sizes) should be carefully considered. Third, our results neglect the influence of motion artifacts inherent to *in vivo* scanning. Fourth, the use of embalmed cadavers without the entirety of surrounding soft tissue also presents differences in the background attenuations as compared to data acquisition *in vivo*.

In conclusion, our findings showed good agreement in Ct.Po between SR-μCT and HR-pQCT using all methods (threshold, density and inhomogeneity). However, the density inhomogeneity method, proposed by Iori et al. [10], with optimized equation indicated no bias and predicted 91% of variance in the SR-μCT derived porosity and therefore appeared as the most appropriate method for estimating Ct.Po using HR-pQCT. These findings can be used to guide future research requiring accurate estimates of Ct.Po for early detection of bone micro-architectural deterioration associated with osteoporosis, for assessing the efficacy of therapies for osteoporosis prevention and treatment, as well as for monitoring growth- and aging-related changes in bone micro-architecture.

Competing interest statement

The authors have no competing interests to declare.

Funding sources

This work was supported in parts by grants from the Natural Sciences and Engineering Research Council (NSERC), Canadian Institutes of Health Research (CIHR) and the Saskatchewan Health Research Foundation (SHRF).

Acknowledgements

The authors wish to acknowledge the anonymous men and women who donated their bodies to science and The Body Bequeathal program, administered by the Department of Anatomy and Cell Biology in the College of Medicine, University of Saskatchewan. The authors also wish to acknowledge the support of the Canadian Light Source and Biomedical Imaging and Therapy facilities and thank the staff in assisting in the SR-μCT data collection. This project was funded in parts through the grants from the Natural Sciences and Engineering Research Council (NSERC), the Canadian Institutes of Health Research (CIHR) and the Saskatchewan Health Research Foundation (SHRF).

References

[1] Y. Bala, R. Zebaze, E. Seeman, Role of cortical bone in bone fragility, Curr. Opin. Rheumatol. 27 (4) (2015) 406–413.
[2] K.S. Davison, K. Siminoski, J.D. Adachi, D.A. Hanley, D. Goltzman, A.B. Hodsman, R. Josse, S. Kaiser, W.P. Olszynski, A. Papaioannou, L.G. Ste-Marie, D.L. Kendler, A. Tenenhouse, J.P. Brown, Bone strength: the whole is greater than the sum of its parts, Semin. Arthritis Rheum. 36 (1) (2006) 22–31.
[3] A.J. Burghardt, G.J. Kazakia, S. Ramachandran, T.M. Link, S. Majumdar, Age- and gender-related differences in the geometric properties and biomechanical significance of intracortical porosity in the distal radius and tibia, J. Bone Miner. Res. 25 (5) (2010) 983–993.
[4] D.M. Cooper, C.E. Kawalilak, K. Harrison, B.D. Johnston, J.D. Johnston, Cortical bone porosity: what is it, why is it important, and how can we detect it? Curr. Osteoporos. Rep. 14 (5) (2016) 187–198.
[5] K.K. Nishiyama, H.M. MacDonald, H.R. Buie, D.A. Hanley, S.K. Boyd, Postmenopausal women with osteopenia have higher cortical porosity and thinner cortices at the distal radius and tibia than women with normal aBMD: an in vivo HR-pQCT study, J. Bone Miner. Res. 25 (4) (2010) 882–890.
[6] H.R. Buie, G.M. Campbell, R.J. Klinck, J.A. MacNeil, S.K. Boyd, Automatic segmentation of cortical and trabecular compartments based on a dual threshold technique for in vivo micro-CT bone analysis, Bone 41 (4) (2007) 505–515.
[7] X.S. Liu, X.H. Zhang, K.K. Sekhon, M.F. Adams, D.J. McMahon, J.P. Bilezikian, E. Shane, X.E. Guo, High-resolution peripheral quantitative computed tomography can assess microstructural and mechanical properties of human distal tibial bone, J. Bone Miner. Res. 25 (4) (2010) 746–756.
[8] B.L. Jorgenson, H.R. Buie, D.D. McErlain, C. Sandino, S.K. Boyd, A comparison of methods for in vivo assessment of cortical porosity in the human appendicular skeleton, Bone 73 (2015) 167–175.
[9] R. Zebaze, A. Ghasem-Zadeh, A. Mbala, E. Seeman, A new method of segmentation of compact-appearing, transitional and trabecular compartments and quantification of cortical porosity from high resolution peripheral quantitative computed tomographic images, Bone 54 (1) (2013) 8–20.
[10] G. Iori, F. Heyer, V. Kilappa, C. Wyers, P. Varga, J. Schneider, M. Grasel, R. Wendlandt, R. Barkmann, J.P. van den Bergh, K. Raum, BMD-based assessment of local porosity in human femoral cortical bone, Bone 114 (2018) 50–61.
[11] W. Tjong, G.J. Kazakia, A.J. Burghardt, S. Majumdar, The effect of voxel size on high-resolution peripheral computed tomography measurements of trabecular and cortical bone microstructure, Med. Phys. 39 (4) (2012) 1893–1903.
[12] G. Margaritondo, R. Meuli, Synchrotron radiation in radiology: novel X-ray sources, Eur. Radiol. 13 (12) (2003) 2633–2641.
[13] V. Bousson, F. Peyrin, C. Bergot, M. Hausard, A. Sautet, J.D. Laredo, Cortical bone in the human femoral neck: three-dimensional appearance and porosity using synchrotron radiation, J. Bone Miner. Res. 19 (5) (2004) 794–801.
[14] Y. Carter, C.D. Thomas, J.G. Clement, A.G. Peele, K. Hannah, D.M. Cooper, Variation in osteocyte lacunar morphology and density in the human femur–a synchrotron radiation micro-CT study, Bone 52 (1) (2013) 126–132.
[15] S. Nuzzo, M.H. Lafage-Proust, E. Martin-Badosa, G. Boivin, T. Thomas, C. Alexandre, F. Peyrin, Synchrotron radiation microtomography allows the analysis of three-dimensional microarchitecture and degree of mineralization of human iliac crest biopsy specimens: effects of etidronate treatment, J. Bone Miner. Res. 17 (8) (2002) 1372–1382.
[16] A. Ostertag, F. Peyrin, S. Fernandez, J.D. Laredo, M.C. de Vernejoul, C. Chappard, Cortical measurements of the tibia from high resolution peripheral quantitative computed tomography images: a comparison with synchrotron radiation micro-computed tomography, Bone 63 (2014) 7–14.
[17] A.H. Holmberg, O. Johnell, P.M. Nilsson, J. Nilsson, G. Berglund, K. Akesson, Risk factors for fragility fracture in middle age. A prospective population-based study of 33,000 men and women, Osteoporos. Int. 17 (7) (2006) 1065–1077.
[18] T.L. Mueller, D. Christen, S. Sandercott, S.K. Boyd, B. van Rietbergen, F. Eckstein, E.M. Lochmuller, R. Muller, G.H. van Lenthe, Computational finite element bone mechanics accurately predicts mechanical competence in the human radius of an elderly population, Bone 48 (6) (2011) 1232–1238.
[19] S. Bonaretti, S. Majumdar, T.F. Lang, S. Khosla, A.J. Burghardt, The comparability of HR-pQCT bone measurements is improved by scanning anatomically standardized regions, Osteoporos. Int. 28 (7) (2017) 2115–2128.
[20] C.E. Kawalilak, J.D. Johnston, D.M. Cooper, W.P. Olszynski, S.A. Kontulainen, Role of endocortical contouring methods on precision of HR-pQCT-derived cortical micro-architecture in postmenopausal women and young adults, Osteoporos. Int. 27 (2) (2016) 789–796.
[21] W.B. Edwards, K.L. Troy, Finite element prediction of surface strain and fracture strength at the distal radius, Med. Eng. Phys. 34 (3) (2012) 290–298.
[22] C.E. Kawalilak, J.D. Johnston, W.P. Olszynski, S.A. Kontulainen, Characterizing microarchitectural changes at the distal radius and tibia in postmenopausal women using HR-pQCT, Osteoporos. Int. 25 (8) (2014) 2057–2066.
[23] J. Schindelin, I. Arganda-Carreras, E. Frise, V. Kaynig, M. Longair, T. Pietzsch, S. Preibisch, C. Rueden, S. Saalfeld, B. Schmid, J.Y. Tinevez, D.J. White, V. Hartenstein, K. Eliceiri, P. Tomancak, A. Cardona, Fiji: an open-source platform for biological-image analysis, Nat. Methods 9 (7) (2012) 676–682.
[24] M.N. Coleman, M.W. Colbert, Technical note: CT thresholding protocols for taking measurements on three-dimensional models, Am. J. Phys. Anthropol. 133 (1) (2007) 723–725.
[25] R.J. Fajardo, T.M. Ryan, J. Kappelman, Assessing the accuracy of high-resolution X-ray computed tomography of primate trabecular bone by comparisons with histological sections, Am. J. Phys. Anthropol. 118 (1) (2002) 1–10.
[26] S. Hansen, V. Shanbhogue, L. Folkestad, M.M. Nielsen, K. Brixen, Bone microarchitecture and estimated strength in 499 adult Danish women and men: a cross-sectional, population-based high-resolution peripheral quantitative computed tomographic study on peak bone structure, Calcif. Tissue Int. 94 (3) (2014) 269–281.
[27] A. Laib, P. Ruegsegger, Comparison of structure extraction methods for in vivo trabecular bone measurements, Comput. Med. Imaging Graph. 23 (2) (1999) 69–74.